Cbf11 and Mga2 function as a single regulatory entity to activate transcription of lipid metabolism genes and promote mitotic fidelity in fission yeast

Running title: Joint functioning of Cbf11 and Mga2

Anna Marešová[1], Michaela Grulyová[1], Miluše Hradilová[2], Viacheslav Zemlianski[1], Jarmila Princová[1], Martin Převorovský[1,*]

[1] Department of Cell Biology, Faculty of Science, Charles University, Viničná 7, 128 00 Prague 2, Czechia

[2] Laboratory of Genomics and Bioinformatics, Institute of Molecular Genetics of the Czech Academy of Sciences, Vídeňská 1083, 142 20 Prague 4, Czechia

* corresponding author; prevorov@natur.cuni.cz

Keywords: lipid metabolism, regulation of transcription, mitotic fidelity, Mga2, CSL proteins, fungi

SUMMARY STATEMENT

Cbf11 and Mga2, transcriptional activators of non-sterol lipid metabolism genes, function as a single regulatory unit and are both required for proper cell cycle progression in the fission yeast *Schizosaccharomyces pombe*.

ABSTRACT

Within a eukaryotic cell, both lipid homeostasis and faithful cell cycle progression are meticulously orchestrated. The fission yeast *Schizosaccharomyces pombe* provides a powerful platform to study the intricate regulatory mechanisms governing these fundamental processes. In *S. pombe*, the Cbf11 and Mga2 proteins are transcriptional activators of non-sterol lipid metabolism genes, with Cbf11 also known as a cell cycle regulator. Despite sharing a common set of target genes, little was known about their functional relationship. This study reveals that Cbf11 and Mga2 function together as a single regulatory entity critical for both lipid metabolism and mitotic fidelity. Deletion of either gene results in a similar array of defects, including slow growth, dysregulated lipid homeostasis, impaired cell cycle progression (cut phenotype), abnormal cell morphology, perturbed transcriptomic and proteomic profiles, and compromised response to the stressors camptothecin and thiabendazole. Remarkably, the double deletion mutant does not exhibit a more severe phenotype compared to the single mutants, suggesting that Cbf11 and Mga2 work together in the same pathway. In addition, ChIP-nexus analysis reveals that both Cbf11 and Mga2 bind to nearly identical positions within the promoter regions of target genes. Interestingly, Mga2 binding appears to be dependent on the presence of Cbf11 and Cbf11 likely acts as a tether to DNA, while Mga2 is needed to activate the target genes. In addition, the study explores the distribution of Cbf11 and Mga2 homologs across fungi. The presence of both Cbf11 and Mga2 homologs in Basidiomycota contrasts with Ascomycota, which mostly lack Cbf11 but retain Mga2. This suggests an evolutionary rewiring of the regulatory circuitry governing lipid metabolism and mitotic fidelity. In conclusion, this study offers compelling support for Cbf11 and Mga2 functioning jointly as a single regulator of lipid metabolism and mitotic fidelity in fission yeast.

INTRODUCTION

Lipids are major constituents of cells, serving as energy reserves and membrane building blocks. In addition, they also have more specialized functions, e.g. in protein modification or as signaling molecules (Hapala et al., 2020; Holič et al., 2020). In yeasts, neutral lipids (triacylglycerols and steryl esters) are stored in cytoplasmic bodies called lipid droplets (LDs). LDs are generated from the endoplasmic reticulum and their hydrophobic lipid core is enclosed in a phospholipid monolayer with associated proteins (Meyers et al., 2016; Meyers et al., 2017). When needed, neutral lipids can be mobilized from LDs to produce phospholipids or to enter energy-generating pathways (Hapala et al., 2020; Holič et al., 2020).

The metabolism of lipids is regulated at multiple levels. In the fission yeast *Schizosaccharomyces pombe*, the phosphatidic acid phosphatase lipin (Ned1) serves as a switch between the production of neutral triglycerides and phospholipids, and thus plays a key role in regulating the production of new membranes (Makarova et al., 2016). This is especially critical in species undergoing closed mitosis, where rapid expansion of the nuclear envelope takes place during anaphase (Yam et al., 2011), and this expansion needs to be supported by sufficient phospholipid production (Foo et al., 2023; Makarova et al., 2016; Takemoto et al., 2016). When these requirements are not met, a catastrophic mitosis leading to the ‘cut’ phenotype can occur, with the undivided nucleus being untimely transected by the division septum (Takemoto et al., 2016; Yam et al., 2011; Yanagida, 1998; Zach and Převorovský, 2018).

At the transcriptional level, lipid homeostasis is maintained by two distinct regulatory branches. Sterol metabolism genes are activated by the membrane-tethered Sre1 transcription factor from the SREBP (sterol regulatory element binding protein) family. Sre1, the homolog of mammalian SREBP-2, is cleaved and activated upon sterol depletion or under hypoxia (Hughes et al., 2005; Lee et al., 2011). On the other hand, triglyceride metabolism genes are regulated by the Mga2 and Cbf11 transcription factors. Mga2, a functional analog of mammalian SREBP-1, is also expressed as a membrane-bound precursor in the endoplasmic reticulum and gets cleaved and activated upon fatty acid shortage or under hypoxia (Burr et al., 2016). Interestingly, the budding yeast *Saccharomyces cerevisiae* contains two paralogs, Mga2p and Spt23p, which also regulate lipid metabolism genes (Chellappa et al., 2001). Cbf11 belongs to the CSL (CBF1/Suppressor of Hairless/LAG-1) transcription factor family and it is a nuclear DNA-binding protein (Převorovský et al., 2009). *S. pombe* cells lacking the *cbf11* gene display pleiotropic defects, including downregulated expression of fatty acid synthesis genes, aberrant LD content, and increased incidence of the ‘cut’ phenotype (Převorovský et al., 2009; Převorovský et al., 2015). Notably, CSL family members are absent from the budding yeast (Převorovský et al., 2007). Intriguingly, there is crosstalk between the sterol and triglyceride regulatory branches, as both Sre1 and Mga2 activation is regulated by the abundance of products of the other branch (Burr et al., 2017).

The Cbf11 and Mga2 regulators have been described independently, but have been shown to display some overlapping functions. Namely, they share a common set of lipid-related target genes, such as the *cut6* acetyl-CoA carboxylase and *ole1* acyl-CoA desaturase, and deletion mutants in both genes show impaired growth and sensitivity to hypoxia (Burr et al., 2016; Převorovský et al., 2009; Převorovský et al., 2015). Despite these similarities, little is known about whether and how these two proteins cooperate. The aim of this study is to explore the functional relationship between Cbf11 and Mga2 in the transcriptional regulation of lipid metabolism, and in promoting mitotic fidelity. Importantly, our results demonstrate that Cbf11 and Mga2 are not independent regulators, but rather function as a single regulatory entity.

RESULTS

Cells lacking the *cbf11* and/or *mga2* gene display similar, non-additive growth and cellular defects

Deletion of the *cbf11* or *mga2* transcription factor gene leads to impaired growth (Burr et al., 2016; Převorovský et al., 2009). Moreover, we have recently shown that both *Δcbf11* and *Δmga2* mutants exhibit increased expression of stress genes and are resistant to H_2O_2 (Princová et al., 2023). To investigate any potential genetic interactions between *cbf11* and *mga2*, we first created *Δcbf11* and *Δmga2* single, and *Δmga2 Δcbf11* double deletion strains in an isogenic background. As expected, the new single deletion strains showed the previously reported growth defects. Interestingly, these growth defects were not additive as the *Δmga2 Δcbf11* double deletion strain did not show any further exacerbation of slow growth when cultured in the complex YES medium (Fig. S1). Previously, we showed that numerous defects of *Δcbf11* cells, including growth defects, are nutrient-dependent and can be suppressed by cultivation in the minimal EMM medium, in which ammonium chloride is the nitrogen source (Převorovský et al., 2015; Zach et al., 2018). Therefore, we asked whether the growth of *mga2* cells also responds to nutrients. Indeed, the doubling time of both *Δmga2* and *Δmga2 Δcbf11* cultures was also reduced in EMM, in a manner similar to *Δcbf11* cells (Fig. S1).

Cbf11 and its DNA-binding activity are required for orderly cell cycle progression. Cells lacking the *cbf11* gene or cells with a point mutation that disrupts DNA binding of Cbf11 (*cbf11DBM*) exhibit various cellular and nuclear defects, such as the 'cut' phenotype, fragmented nuclear mass, aberrant septation and/or cell separation (Marešová et al., 2024; Převorovský et al., 2009). Therefore, we next determined whether any such defects were also present in cells lacking *mga2*. To this end, we analyzed WT, *Δcbf11*, *Δmga2*, and *Δmga2 Δcbf11* cells stained with DAPI by microscopy. Strikingly, the *Δmga2* mutant largely recapitulated the morphological and cell-cycle defects of the *Δcbf11* cells (Fig. 1A, B). Interestingly, the incidence of the 'cut' phenotype in the double deletion mutant was not further increased compared to the single mutants (Fig. 1B). In summary, we have shown that disruption of

either of the two transcriptional activators of lipid metabolism genes leads to cell-cycle defects, and these are not additive in the *Δmga2 Δcbf11* double mutant.

Cells lacking the *cbf11* or *mga2* gene display similar transcriptomic and proteomic signatures

To examine the possible joint functioning of Cbf11 and Mga2, we first determined the transcript levels of their selected target genes in *Δcbf11*, *Δmga2*, and *Δmga2 Δcbf11* cells by RT-qPCR. The panel of tested genes included *cut6* (acetyl-CoA carboxylase), *ole1* (acyl-CoA desaturase), *lcf1* and *lcf2* (long-chain fatty acid-CoA ligases), *fsh2* (serine hydrolase-like), *vht1* (biotin transporter), *bio2* (biotin synthase) and *fas2* (fatty acid synthase alpha subunit). We observed that all tested genes were significantly downregulated in both single mutants compared to WT (Fig. 2A). Interestingly, the decrease in transcript levels in the double deletion mutant was not additive compared to the single mutants (Fig. 2A). Next, we confirmed and extended these results by an RNA-seq analysis (Fig. 2B, Fig. S2). We found a strong overlap between the sets of differentially expressed genes (DEGs) in the *Δcbf11* and *Δmga2* single mutants (Fig. 2C). In addition, the double deletion mutant showed a transcriptomic profile almost identical to *Δmga2* (Fig. 2C).

We have previously shown that deletion of the *cbf11* gene or disabling Cbf11 binding to DNA (Cbf11DBM) leads to upregulation of many non-coding RNAs ((Marešová et al., 2024); Fig. 2E). We wanted to know whether this phenotype is specific to the Cbf11 regulator or whether it is more generally related to perturbed lipid metabolism. To this end we analyzed the non-coding transcriptomes of *Δcbf11*, *Δmga2*, and *Δmga2 Δcbf11* cells, and also included the *Pcut6MUT* lipid metabolism mutant, and WT cells treated with cerulenin. In the *Pcut6MUT* strain, the *cut6* promoter lacks the Cbf11 binding site and *cut6* expression drops to 50% (Převorovský et al., 2016), while cerulenin is a fatty acid synthase inhibitor. Strikingly, we found very similar deregulation of the non-coding transcriptome in all tested mutants and treatments (Fig. 2E). Thus, we conclude that unperturbed lipid metabolism is required for correct expression of the non-coding transcriptome.

Finally, since the absence of either the *cbf11* or *mga2* gene resulted in similar transcriptome changes, we decided to also compare the proteomes of the *Δcbf11* and *Δmga2* mutants using untargeted mass spectrometry. This analysis revealed a dramatic overlap of proteins that were expressed differentially in the respective single mutants compared to WT (Fig. 2D). Taken together, these results strongly suggest that the functions of Cbf11 and Mga2 are very closely related.

Cbf11 and Mga2 have overlapping roles in maintaining lipid homeostasis

Cbf11-deficient cells show an overall reduction in the abundance of lipid droplets (LDs) and pronounced cell-to-cell LD heterogeneity when grown in YES (Marešová et al., 2024; Převorovský et al., 2015). Both these phenotypes are rescued by growing the mutant cells in EMM (Zach et al., 2018). Therefore, we now also analyzed LD content in the *Δmga2* single, and *Δmga2 Δcbf11* double deletion mutants (Fig.

3). Similar to the *Δcbf11* mutant, we observed a decrease in LD content (in both LD staining intensity and LD number per unit of cell volume; Fig. 3B, C), and marked LD content heterogeneity in cultures lacking Mga2 grown in YES (Fig. 3A). Notably, the defects were not further exacerbated in the double mutant. Furthermore, in all mutants the defects were largely suppressed when cells were grown in EMM. So, once again, the phenotypes of the *Δcbf11* and *Δmga2* mutants were very similar and were non-additive, suggesting joint functioning of Cbf11 and Mga2 in lipid homeostasis.

Cbf11 and Mga2 are both required for genome integrity

We have recently described a requirement for Cbf11 in the maintenance of chromatin structure and genome integrity. Cells lacking intact Cbf11 are sensitive to the microtubule poison thiabendazole (TBZ), and to camptothecin (CPT), an inhibitor of topoisomerase II and a potent inducer of double-stranded DNA breaks (Marešová et al., 2024; Vishwanatha et al., 2023). We now tested whether Mga2 is also involved in these processes. Indeed, both *Δmga2* and *Δmga2 Δcbf11* mutants showed sensitivities to TBZ and CPT similar to the *Δcbf11* mutant (Fig. 4). So far, our analyses revealed that the *Δmga2* mutant is very similar to *Δcbf11* cells, and that the phenotypes of the *Δmga2 Δcbf11* double mutant are non-additive. Therefore, our results strongly suggest joint functioning of Cbf11 and Mga2 in a range of cellular processes.

Cbf11 and Mga2 share DNA binding sites

We have recently mapped Cbf11 binding sites using the genome-wide ChIP-nexus technique (Marešová et al., 2024), which can determine the target protein footprint on DNA at a much higher resolution compared to traditional ChIP-seq (He et al., 2015). Since Mga2 is also presumed to be a DNA-binding transcription factor, we set out to conduct a ChIP-nexus analysis for Mga2 as well. Cbf11 and Mga2 regulate a highly overlapping set of genes ((Burr et al., 2016; Převorovský et al., 2015); Fig. 2), so we were especially interested in determining how this joint regulation is carried out. Cbf11 is known to be able to bind DNA directly (Oravcová et al., 2013). Therefore, we considered the following three scenarios (Fig. 5A): a) Cbf11 and Mga2 bind to target promoter DNA individually and independently of each other, b) they bind DNA together as a complex, with each protein contacting the promoter via its own DNA-binding domain, c) they bind DNA together as a complex, with Cbf11 serving as the DNA-binding subunit. To avoid as many confounding variables as possible, we used isogenic scarless TAP knock-in strains constructed using CRISPR/Cas9. The C-terminally tagged Cbf11-TAP strain has been described previously (Marešová et al., 2024; Princová et al., 2023). Inactive, membrane-bound Mga2 undergoes proteolytic activation that liberates its N-terminal part, which can then regulate transcription in the nucleus (Burr et al., 2017). Therefore, the TAP tag was fused to the N-terminus in the case of Mga2. Next, we also deleted the *cbf11* and *mga2* gene in the TAP-Mga2 and Cbf11-TAP background, respectively, to allow for assessing the interdependence of Cbf11 and Mga2 for binding to DNA. We confirmed that the introduction of the TAP tag had no adverse effect on the growth rate. The growth of the TAP-Mga2 *Δcbf11* strain was only slightly slower compared to untagged

Δcbf11, while the growth of the Cbf11-TAP *Δmga2* strain was comparable to the growth of untagged *Δmga2* (Fig. S3).

Subsequent ChIP-nexus analysis revealed that the exact positions of the binding sites of Cbf11 and Mga2 in the promoters of most lipid metabolism genes overlap closely and show very similar footprints (Fig. 5B, S4). Moreover, the binding of Mga2 to DNA at most sites was dependent on Cbf11, as Mga2 in the *Δcbf11* background did not bind to the promoters of *cut6*, *ole1* (Fig. 5B), *lcf2*, *ptl1*, *fsh2* and *vht1* (Fig. S4A). Nevertheless, we also observed cases where the Cbf11 and Mga2 binding patterns were different (Fig. S4B): a) Mga2 binding to the *lcf1* promoter was Cbf11-dependent, but then the absence of Mga2 resulted in markedly reduced binding and an altered footprint of Cbf11, b) both Cbf11 and Mga2 binding to the *fas1* promoter was fully dependent on the presence of the other counterpart, c) the *ptl2* promoter was bound by Cbf11 or Mga2 regardless of the presence of the other protein, even though the occupancy was reduced when the other protein was missing. We also found that the promoters of *bio2* and *fas2*, genes whose expression is Cbf11 and Mga2 dependent (Fig. 2A, B), were not bound by Cbf11 or Mga2 proteins at all, suggesting indirect regulation (Fig. S4C). Overall, although we observed several different binding arrangements, the majority of target promoters showed closely overlapping binding profiles of Cbf11 and Mga2, and this binding to DNA was dependent on Cbf11.

Finally, we compared the Cbf11 and Mga2 ChIP-nexus results with results of transcriptome analyses of *Δcbf11* and *Δmga2* deletion mutants. We found that binding of Cbf11 and Mga2 to the promoters of numerous genes of lipid metabolism (*cut6, ole1, lcf1, lcf2, fsh2, vht1, ptl2, fas1*; Fig. 5B, S4A, S4B) correlated with reduced transcript levels of these genes when either *cbf11* or *mga2* was deleted (Fig. 2A, 2B, S2). Thus, while Cbf11 can bind the target promoters on its own, the presence of Mga2 is then required to bring about changes in target gene transcription. Taken together, these results are compatible with a scenario where Cbf11 and Mga2 form a complex that activates the expression of lipid metabolism genes. In this hypothetical complex, Cbf11 would serve as the DNA-binding subunit, while Mga2 would serve as the transcription activation subunit (see Fig. 5A, bottom scenario).

Mga2 has both CSL-dependent and independent functions in Fungi

All our results so far indicated that Cbf11 and Mga2 function together as one regulatory entity in *S. pombe*. Curiously, the budding yeast *Saccharomyces cerevisiae* is known to contain two Mga2 homologs (Mga2p and Spt23p; (Chellappa et al., 2001)), while no CSL family members are present (Převorovský et al., 2007). Similar to *S. pombe*, the budding yeast Mga2p/Spt23p are also implicated in regulating lipid metabolism genes such as the fatty acid desaturase *OLE1* (Chellappa et al., 2001), suggesting that Mga2 homologs can also function in a CSL-independent manner. To gain more insight into the evolutionary rewiring of the Mga2-CSL circuitry, we examined the phylogenetic distribution of these two protein families within the Fungi kingdom. Using the protein sequences of *S. pombe* Cbf11 and Mga2 as queries, we found 109 taxons that contained both Cbf11 and Mga2 homologs, 386 taxons that contained only Mga2 homolog(s), and 1 taxon that contained only Cbf11 homolog(s) (Table S5). A

phylogenetic tree was then generated from all identified taxons (Fig. 6) to assess the distribution of Cbf11 and Mga2 homologs.

We found that in the Basidiomycota phylum the CSL and Mga2 families co-occur in most taxons (Fig. 6). The only exceptions were one species from the Ustilaginomycotina subdivision (*Ceraceosorus guamensis*) that apparently lacks Mga2 homologs, and two species from the Agaricomycotina subdivision (*Tremella mesenterica* and *Mycena indigotica*) that do not seem to contain any Cbf11 homologs. However, these rare exceptions may be false negatives and merely reflect potential errors in genome assembly of the respective species. By contrast, the CSL/Mga2 distribution was markedly different in the Ascomycota phylum. Here, Mga2 homologs were universally present, but Cbf11 homologs were typically absent (Fig. 6). More specifically, CSL proteins were only found in several species belonging to the Taphrinomycotina subdivision. These included members of the class *Schizosaccharomycetes* (*Schizosaccharomyces pombe*, *S. japonicus*, *S. octosporus*, *S. cryophilus*, *S. osmophilus*), the class Pneumocystidomycetes (*Pneumocystis murina*, *P. jirovecii*, *P. carinii*), and the class Taphrinomycetes (*Protomyces lactucae-debilis* and *Saitoella complicata*). Our results thus suggest that in fungi Cbf11 homologs occur and likely also function (almost) exclusively together with Mga2 homologs, whereas Mga2 proteins can operate independently of the CSL protein family.

DISCUSSION

Mga2 and the CSL family transcription factor Cbf11 are currently the only known transcriptional regulators of fatty acid and triacylglycerol metabolism in the fission yeast *S. pombe* (Burr et al., 2016; Převorovský et al., 2016). They were shown to regulate a common set of genes (Burr et al., 2016; Převorovský et al., 2015), but nothing was known about the potential functional interactions between Mga2 and Cbf11. To decipher the relationship between Cbf11 and Mga2, we now subjected strains lacking *cbf11* and/or *mga2* to extensive functional analyses. In all test cases, the behavior of *Δmga2* corresponded to the phenotype of *Δcbf11*. Moreover, the double deletion mutant did not show an additive phenotype. We showed that the positions of the Cbf11 and Mga2 binding sites closely overlap in most promoters of their target lipid metabolism genes. Typically, Mga2 cannot bind to DNA in the absence of Cbf11. On the other hand, Cbf11 can bind to DNA on its own, but it cannot activate transcription without Mga2. Thus, our results demonstrate that Cbf11 and Mga2 function together as DNA-binding and transcription activation components, respectively, of a single regulatory entity. Finally, we have established Mga2 as a novel regulator of mitotic progression, as *Δmga2* cells are prone to the 'cut' catastrophic mitosis.

The data we gathered strongly suggested that Cbf11 and Mga2 form a protein complex. Also, Mga2 was shown previously to co-purify with Cbf11-TAP in a one-step IgG-based pull-down followed by mass spectrometry (Pancaldi et al., 2012). However, in the current study we failed to detect a physical interaction between Cbf11 and Mga2, despite using a range of affinity purification approaches of both

endogenous and heterologously expressed proteins. We suspect this may be a false negative result caused by the low abundance of both proteins (hundreds of molecules per cell; (Carpy et al., 2014; Marguerat et al., 2012)) or their susceptibility to proteolysis (Převorovský et al., 2011). Also, the hypothetical physical interaction between Cbf11 and Mga2 may be too transient to be detected by biochemical purifications. To confirm the suspected Cbf11-Mga2 physical interaction, future studies could therefore employ alternative methods such as proximity-dependent biotinylation assay (TurboID; (Larochelle et al., 2019)), fluorescence resonance energy transfer (FRET; (Skruzny et al., 2019)), or the yeast two-hybrid system (Selicky et al., 2022).

The production, utilization and/or storage of various lipid types needs to adapt to factors such as nutrient availability, population density, osmotic pressure, ambient temperature, etc. (Hapala et al., 2020; Holič et al., 2020). It is conceivable that Cbf11 and Mga2 activities are coupled to these environmental cues to achieve proper lipid homeostasis. Indeed, Mga2 is required for growth under hypoxic conditions, where low oxygen availability limits the process of fatty acid desaturation, thereby affecting membrane rigidity and vesicle trafficking (Burr et al., 2017). Interestingly, the proteolytic activation of the membrane-bound Mga2 precursor is triggered by fatty acid shortage, and Mga2 activity was also found to be cross-regulated by the Sre1/SREBP-dependent sterol synthesis pathway (Burr et al., 2017). Moreover, cells lacking Cbf11 are sensitive to low temperatures (Převorovský et al., 2009), a condition where proper adjustments of membrane composition are critical for survival. Finally, we have shown previously (Zach et al., 2018; Zemlianski et al., 2023) and also in the present study that Cbf11 and Mga2 activities are affected by nitrogen availability. A well-utilizable nitrogen source activates the Tor2 kinase, a major growth regulator of *S. pombe* (Hartmuth and Petersen, 2009). Intriguingly, both Cbf11 and Mga2 are phosphorylated at multiple sites (Carpy et al., 2014; Kettenbach et al., 2015; Koch et al., 2011), and the phosphorylation at S505 and T1091 of Mga2 is actually TOR-dependent (Mak et al., 2021). On top of that, Cbf11 and Mga2 are sumoylated at K89 and K615, respectively (Køhler et al., 2015); Mga2 is glycosylated at N17 and N998 (Zielinska et al., 2012), and ubiquitinated at multiple positions (Beckley et al., 2015; Strachan et al., 2023). While the biological significance of these numerous posttranslational modifications remains unknown, they represent plausible means of regulating Cbf11-Mga2 protein abundance and activity. Indeed, ubiquitination at specific lysine residues is important for the proteasome- and Cdc48p ATPase-dependent activation of the Mga2p120 precursor in *Saccharomyces cerevisiae* (Bhattacharya et al., 2009).

Our phylogenetic analyses showed that Mga2 homologs operate in a CSL-independent manner in the vast majority of ascomycetes (Fig. 6). A question thus arises how these Mga2 homologs bind to DNA - do they utilize a CSL-unrelated DNA binding partner, or can they bind to DNA directly? Earlier studies in *S. cerevisiae* identified the LORE (low oxygen response element) DNA motif in the promoter of the *OLE1* fatty acid desaturase gene (Vasconcelles et al., 2001), a regulatory target of Mga2p/Spt23p (Zhang et al., 1999). Notably, the core LORE sequence ACTCAACAA is not reminiscent of the Cbf11 response element CGTG(G/A)GAA. Interestingly, *S. cerevisiae* Mga2p/Spt23p are not thought to be capable of direct DNA binding (Zhang et al., 1997), but a LORE-binding protein complex has been

identified which does contain Mga2p (Jiang et al., 2001). This suggests that ascomycetal Mga2 homologs (with the exception of Taphrinomycotina) serve as transcriptional co-activators that require a yet unidentified DNA-binding partner(s) for accessing target promoters.

It should also be noted that *S. pombe* contains a second CSL protein, Cbf12 (Převorovský et al., 2009), which also functions as a DNA-binding activator of transcription (Kwon et al., 2012; Oravcová et al., 2013; Převorovský et al., 2011). However, Cbf12 has a specialized function in cell adhesion (Kwon et al., 2012; Převorovský et al., 2009), and its deletion does not cause any adverse phenotype under standard growth conditions (Převorovský et al., 2009), unlike in the case of Cbf11 or Mga2. There are currently no indications that Cbf12 cooperates with Mga2, but the exact mechanism of Cbf12-mediated transcription activation, including whether Cbf12 requires a coactivator partner, remains to be established.

Finally, it is intriguing that while the ablation of Cbf11 and/or Mga2 results in a plethora of cellular defects, the Cbf11-Mga2 regulatory entity is not strictly essential for viability, even though it regulates essential genes (such as *cut6*) and processes. This can be explained by the fact that in the absence of Cbf11-Mga2 the expression of their target genes only drops by ~50% (Fig. 2). It is therefore possible, or perhaps even likely, that *S. pombe* possesses additional activator(s) of non-sterol lipid metabolism genes, which act independently and in parallel to Cbf11-Mga2. These remain to be identified by future studies.

MATERIALS AND METHODS

Plasmid construction

The Cas9/sgRNA_*mga2* plasmid (pMP167) was prepared as follows. sgRNA targeted to the *mga2* ORF was inserted into the pLSB plasmid (alternative name pMP160) carrying an empty sgRNA cassette (with a GFP placeholder) and a Cas9 endonuclease gene that is codon-optimized for expression in *S. pombe* (Torres-Garcia et al., 2020). Briefly, a suitable sgRNA targeting the 5' end of the *mga2* ORF was manually designed, 24-nt forward and reverse sgRNA oligonucleotides (AJ89 and AJ90; 20-nt sgRNA with 4-nt *BsaI* overhangs) were annealed, phosphorylated and inserted into the *BsaI*-digested pLSB plasmid.

To create the pMP168 plasmid, the *TAP-mga2** fragment for HR (see Text S1) was cloned into the pBluescript SK(+) plasmid. Briefly, HR template was divided into 3 parts and each part was amplified by NEB Q5 polymerase using AJ51 & AJ52 oligonucleotides for part 1, AJ53 & AJ54 for part 2, and AJ55 & AJ56 for part 3. Genomic DNA from WT cells was used as a template for PCR amplification of HR part 1 and 3. To amplify HR part 2, pMaP27 plasmid containing a TAP-tag sequence was used as template. All three PCR-amplified and purified parts were inserted into the pBluescript SK(+) vector to

create the final pMP168 plasmid. Note that the HR template contains a point mutation (marked as *) that disrupts the PAM sequence in the *mga2* ORF to avoid re-cleavage by Cas9.

Both final plasmids pMP167 and 168 were verified by restriction cleavage and sequencing.

Cultivations, media and strains

Schizosaccharomyces pombe cells were grown at 32°C to exponential phase (OD_{600} = 0.5) according to standard procedures (Petersen and Russell, 2016) in either complex yeast extract medium with supplements (YES) or Edinburgh minimal medium (EMM). Routine optical density (OD) measurements of liquid cell cultures were taken using the WPA CO 8000 Cell Density Meter (Biochrom). Growth rate measurements and calculation of cell culture doubling time (DT) were performed as described previously (Zach et al., 2018).

The construction of the scarless knock-in strain expressing C-terminally TAP-tagged Cbf11 from its endogenous chromosomal locus (Cbf11-TAP) was described previously (Princová et al., 2023).

In this study, we N-terminally TAP-tagged *mga2* at its chromosomal locus to allow detection and distinction between the full-length precursor form and the cleaved active N-terminal transcription factor form of Mga2. To this end, the CRISPR/Cas9-based *SpEDIT* strategy was adapted from (Torres-Garcia et al., 2020). WT cells (JB32) were synchronized in G1 and transformed (Rodríguez-López et al., 2016) with the Cas9/sgRNA_*mga2* plasmid (pMP167) together with a fragment of the *TAP-mga2** sequence (plasmid pMP168 digested by *SacI* and *XhoI*) as template for homologous recombination. The *TAP-mga2** sequence contained a silent mutation which prevented re-cleavage of the tagged *mga2* locus by Cas9. After selection on YES plates containing 100 µg/mL of Nourseothricin (NAT), the smallest NAT-resistant colonies were re-streaked onto non-selective YES plates to allow loss of the Cas9/sgRNA_*mga2* plasmid. Correct integration of the *TAP-mga2** sequence was verified by PCR (primers MaP172 and AJ92) and sequencing. Expression of the TAP-Mga2 protein was verified by western blot with an anti-TAP antibody (Thermo Scientific, CAB1001).

Constructions of the *Δcbf11* and *Δmga2* single deletion strains were published elsewhere (Převorovský et al., 2015; Princová et al., 2023). To create the *Δmga2 Δcbf11*, Cbf11-TAP *Δmga2*, and TAP-Mga2 *Δcbf11* strains, the pClone system was used for deletion of the *cbf11* and/or *mga2* genes (Gregan et al., 2006).

The lists of strains, plasmids and primers used in this study are provided in Table S1, Table S2 and Table S3.

Spot tests

Exponentially growing cell cultures were 10-fold serially diluted and spotted onto control YES plates and testing YES plates containing thiabendazole (TBZ; 15 and 18 µg/mL) or camptothecin (CPT; 4 and 6 µM) for drug sensitivity assays. Plates were imaged after 6 days of incubation at 32˚C. Two independent experiments with technical replicates were performed.

Fluorescence microscopy

Fluorescence microscopy was performed as described previously (Marešová et al., 2024). Briefly, for observation of nuclear morphology and quantification of 'cut' phenotype, nuclei of ethanol-fixed cells were stained with DAPI. 'Cut' cells were counted manually; 200-1000 cells per sample were analyzed. For visualization of lipid droplets (LDs), live cells grown to exponential phase in YES or EMM were stained with BODIPY 493/503. 7-14 images per sample were processed by an automated MATLAB pipeline (Princová et al., 2019). Resulting output data were processed using R. At least six ('cut' counting) or three (LD content) independent experiments were performed. To determine statistical significance, Welch Two Sample t-test was performed on raw data (t.test function in R, paired = FALSE, alternative = "greater" for 'cut' counting, alternative = "less" for LD content).

RT-qPCR

Expression of selected lipid metabolism genes in exponentially growing cells was analyzed as described previously (Marešová et al., 2024). Briefly, total RNA was extracted and converted to cDNA using random priming. qPCR reactions were performed in technical triplicates. For normalization, *act1* (actin) and *rho1* (Rho1 GTPase) were used as internal reference genes. One-sided Mann-Whitney U test was used to determine statistical significance (wilcox.test function in R, paired = FALSE, alternative = "less"). At least three independent biological experiments were performed. The primers used are listed in Table S3.

RNA-seq

RNA-seq analyses for WT (JB32) and *Δcbf11* (MP44) were already published (Marešová et al., 2024). Additional RNA-seq analyses shown in this study were performed as described previously (Marešová et al., 2024). Briefly, *Δmga2* (MP815), *Δmga2 Δcbf11* (MP836), and *Pcut6MUT* (MP636) cells were cultured in YES to exponential phase and harvested. For cerulenin-related analyses, WT cells were grown to exponential phase and treated with DMSO (control) or 20 µM cerulenin for 1 hour in YES and then harvested. Samples were prepared from 3 biological replicates. Total RNA was isolated, treated with TURBO DNase and column-purified. RNA quality was assessed on Agilent Bioanalyzer. Sequencing library construction and sequencing were performed by the Genomics and Bioinformatics service facility at the Institute of Molecular Genetics (Czech Academy of Sciences, Prague) using the

Illumina NextSeq 500 sequencing system. For detailed RNA-seq data analysis please refer to (Marešová et al., 2024).

ChIP-nexus

ChIP-nexus analyses for Cbf11-TAP (MP707) and untagged WT (JB32, a negative control) were already published elsewhere (Marešová et al., 2024). Three independent biological experiments of ChIP-nexus for Cbf11-TAP *Δmga2* (MP921), TAP-Mga2 (MP872), and TAP-Mga2 *Δcbf11* (MP915) presented here were performed and analyzed in the same manner as described previously for Cbf11-related analyses (Marešová et al., 2024). Briefly, cells were cultivated in YES to exponential phase and fixed with 1% formaldehyde followed by quenching in 125 mM glycine. Chromatin was extracted and sheared with the Bioruptor sonicator (Diagenode). For the intended downstream normalization of ChIP samples, 2 mg of each *S. pombe* chromatin were mixed with 40,000-fold diluted *Saccharomyces cerevisiae* chromatin sample containing TAP-tagged version of histone H2A.2 (strain MP792). Note that in the end the spike-in normalization was disregarded during data analyses. Chromatin immunoprecipitation was performed overnight at 4°C with 100 µL of BSA-blocked Pan Mouse IgG Dynabeads (Invitrogen, 110.41). The precipitated material was ChIP-exo treated, decrosslinked, and treated with RNase A and proteinase K. DNA was purified using phenol-chloroform extraction followed by sodium acetate/ethanol precipitation and was used for the subsequent construction of ChIP-nexus sequencing libraries. Sequencing was performed by the Genomics and Bioinformatics service facility at the Institute of Molecular Genetics (Czech Academy of Sciences, Prague) using the Illumina NextSeq 500 sequencing system. The list of used ChIP-nexus oligonucleotides is provided in Table S4. For detailed ChIP-nexus data analysis please refer to (Marešová et al., 2024).

Proteomic analysis

WT (JB32), *Δcbf11* (MP44), and *Δmga2* (MP815) cells were cultured in YES to exponential phase in three independent biological replicates. 20 mL of culture were harvested and the cell pellets were flash-frozen in liquid nitrogen. Samples were processed in the Laboratory of Mass Spectrometry at Biocev Research Center (Faculty of Science, Charles University, Prague), where the bottom-up untargeted proteomic analysis was performed.

To extract proteins, cells were lysed by milling using FastPrep (MP Biomedicals) with glass beads and incubated at 95°C for 10 min in 100 mM Triethylammonium bicarbonate (TEAB) containing 2% sodium deoxycholate (SDC), 40 mM chloroacetamide, and 10 mM Tris(2-carboxyethyl)phosphine (TCEP). Protein concentration was determined using BCA protein assay kit (Thermo Scientific) and 30 µg of protein per sample were further processed using the SP3 technology for protein cleanup and digestion (Hughes et al., 2019). Briefly, 5 µL of SP3 beads were added to protein samples and protein binding was induced by adding ethanol to 60% (vol./vol.) final concentration. Samples were mixed and incubated for 5 min at room temperature. Using a magnetic rack, the unbound material was discarded

and the beads were subsequently washed with 80% ethanol. Next, samples were digested with trypsin (1:30 enzyme to protein ratio) and reconstituted in 100 mM TEAB at 37°C overnight. The resulting peptide samples were acidified with trifluoroacetic acid (1% final concentration), desalted using in-house stage tips packed with C18 disks (Empore) according to (Rappsilber et al., 2007), and subjected to nano-liquid chromatography coupled to tandem mass spectrometry (nLC-MS2) analysis (Hebert et al., 2014). Nano Reversed phase columns (EASY-Spray column, 50 cm x 75 µm ID, PepMap C18, 2 µm particles, 100 Å pore size) were used. Mobile phase buffer A was composed of water and 0.1% formic acid. Mobile phase B was composed of acetonitrile and 0.1% formic acid. Samples were loaded onto the trap column (C18 PepMap100, 5 µm particle size, 300 µm x 5 mm, Thermo Scientific) for 4 min at 18 µL/min. Loading buffer was composed of water, 2% acetonitrile and 0.1% trifluoroacetic acid. Peptides were eluted with Mobile phase B gradient from 4% to 35% B in 60 min. Eluting peptide cations were converted to gas-phase ions by electrospray ionization and analyzed on a Thermo Orbitrap Fusion (Q-OT-qIT, Thermo Scientific). Survey scans of peptide precursors from 350 to 1400 *m/z* were performed in orbitrap at 120K resolution (at 200 *m/z*) with a 5×10^5 ion count target. Tandem MS was performed by isolation at 1.5 Th with the quadrupole, HCD fragmentation with normalized collision energy of 30, and rapid scan MS analysis in the ion trap. The MS2 ion count target was set to 10^4 and the max injection time was 35 ms. Only those precursors with charge state 2–6 were sampled for MS2. The dynamic exclusion duration was set to 45 s with a 10 ppm tolerance around the selected precursor and its isotopes. Monoisotopic precursor selection was turned on. The instrument was run in top speed mode with 2 s cycles.

All data were analyzed and quantified with the MaxQuant software (version 2.0.3.0) (Cox and Mann, 2008). The false discovery rate (FDR) was set to 1% for both proteins and peptides. A minimum peptide length was specified to seven amino acids. The Andromeda search engine was used for the MS/MS spectra search against the *S. pombe* database (downloaded from uniprot.org). Enzyme specificity was set as C-terminal to Arg and Lys, also allowing cleavage at proline bonds and a maximum of two missed cleavages. Carbamidomethylation of cysteine was selected as a fixed modification and N-terminal protein acetylation and methionine oxidation as variable modifications. The “match between runs” feature of MaxQuant was used to transfer identifications to other LC-MS/MS runs based on their masses and retention time (maximum deviation 0.7 min) and this was also used in quantification experiments. Quantifications were performed with the label-free algorithm in MaxQuant (Cox et al., 2014). Data analysis was performed using Perseus 1.6.15.0 software (Tyanova et al., 2016). Proteins showing at least 2-fold and statistically significant change in expression in *Δcbf11* or *Δmga2* mutants compared to WT were selected for further analyses.

Phylogenetic distribution of Cbf11 and Mga2 homologs

The Protein BLAST (*blastp*) tool (https://blast.ncbi.nlm.nih.gov/Blast.cgi?PROGRAM=blastp&PAGE_TYPE=BlastSearch&LINK_LOC=blasthome) from the National Centre for Biotechnology Information (NCBI) was used to determine the

distribution of Cbf11 and Mga2 homologs among Fungi (taxID: 4751). The *blastp* search was performed using default settings against the Reference sequence database (Refseq_protein; https://www.ncbi.nlm.nih.gov/refseq/; June 22, 2023) with the protein sequences of *S. pombe* Cbf11 (SPCC736.08) and Mga2 (SPAC26H5.05) taken from the PomBase database (https://www.pombase.org/) as queries. In total, 226 sequences were found for the Cbf11 query and 1223 sequences were found for the Mga2 query. These protein sequences were manually filtered to only keep those that showed high-quality alignment in the regions of the known signature domains of Cbf11 (RHR-N and Beta-trefoil) and Mga2 (IPT and Ankyrin repeats). As a result, three lists of taxIDs were compiled: taxons containing both Cbf11 and Mga2 homologs, taxons containing only Cbf11 homolog(s), and taxons containing only Mga2 homolog(s). These lists were visualized in the NCBI Common Taxonomy Tree tool (https://www.ncbi.nlm.nih.gov/Taxonomy/CommonTree/wwwcmt.cgi). Subsequently, the taxons in which homologs from only one of the Cbf11/Mga2 families were originally found were searched by *blastp* individually to confirm the absence of the respective protein family (performed July 2-20, 2023). Thereby, three final taxID lists were created (Cbf11&Mga2, Cbf11_only, Mga2_only). A combined list of all identified taxIDs was used to generate a phylogenetic tree by the NCBI Common Taxonomy Tree and individual taxIDs were assigned the corresponding taxon names using the NCBI TaxIdentifier tool (https://www.ncbi.nlm.nih.gov/Taxonomy/TaxIdentifier/tax_identifier.cgi). iTOL v6 was used to display and annotate the final phylogenetic tree (https://itol.embl.de/). The taxIDs lists with corresponding taxon names are provided in Table S5.

DATA AVAILABILITY

The sequencing data are available from the ArrayExpress database (https://www.ebi.ac.uk/arrayexpress/) under the accession numbers E-MTAB-13303 (RNA-seq of *Δmga2* and *Δmga2 Δcbf11*) and E-MTAB-13305 (RNA-seq of WT, *Pcut6MUT,* WT treated with cerulenin and control WT treated with DMSO).

Previously published sequencing data (Marešová et al., 2024) were obtained from ArrayExpress with the following accession numbers: E-MTAB-13258 for all ChIP-nexus libraries, E-MTAB-13302 and E-MTAB-13305 for RNA-seq of WT and *Δcbf11*.

The scripts used for sequencing data processing and analyses are available from https://github.com/mprevorovsky/RNA-seq_ammonium (WT, *Δcbf11*), https://github.com/mprevorovsky/RNA-seq_CSL-DBM_cerulenin (WT, cerulenin treatment), and https://github.com/mprevorovsky/RNA-seq_mga2 (*Δmga2*, *Δmga2 Δcbf11*).

Source data for Figures, including the numbers of independent experiments (n) in bar plots (Fig. 1B, 2A, 3B, 3C, S1, S3) are available as Supplementary File 2.

FUNDING

This work was supported by the Grant Agency of Charles University (GA UK grant no. 248120 to A.M.). M.H. was supported by the European Union - Next Generation EU (programme EXCELES project no. LX22NPO5102).

ACKNOWLEDGEMENTS

We would like to thank Barbora Huraiová and Silvia Bágeľová-Poláková (Slovak Academy of Science, Bratislava) for providing plasmid DNA, and Marian Novotný for help with interpreting protein 3D structure predictions. We are grateful to Štěpánka Hrdá and Blanka Hamplová from the Genomics core facility at Biocev Research Center, Faculty of Science, Charles University for Sanger sequencing and quality control of nucleic acids; Adéla Kracíková, Kateřina Svobodová and Eva Krellerová for excellent technical assistance; all members of the GenoMik group for their support and insightful discussions. Microscopy was performed in the Vinicna Microscopy Core Facility co-financed by the Czech-BioImaging large RI project LM2023050. Computational resources were supplied by the project "e-Infrastruktura CZ" (e-INFRA LM2018140) provided within the program Projects of Large Research, Development and Innovations Infrastructures. LC-MS analyses were performed in the Laboratory of Mass Spectrometry at Biocev Research Center; Faculty of Science, Charles University.

COMPETING INTERESTS

No competing interests declared.

FIGURES

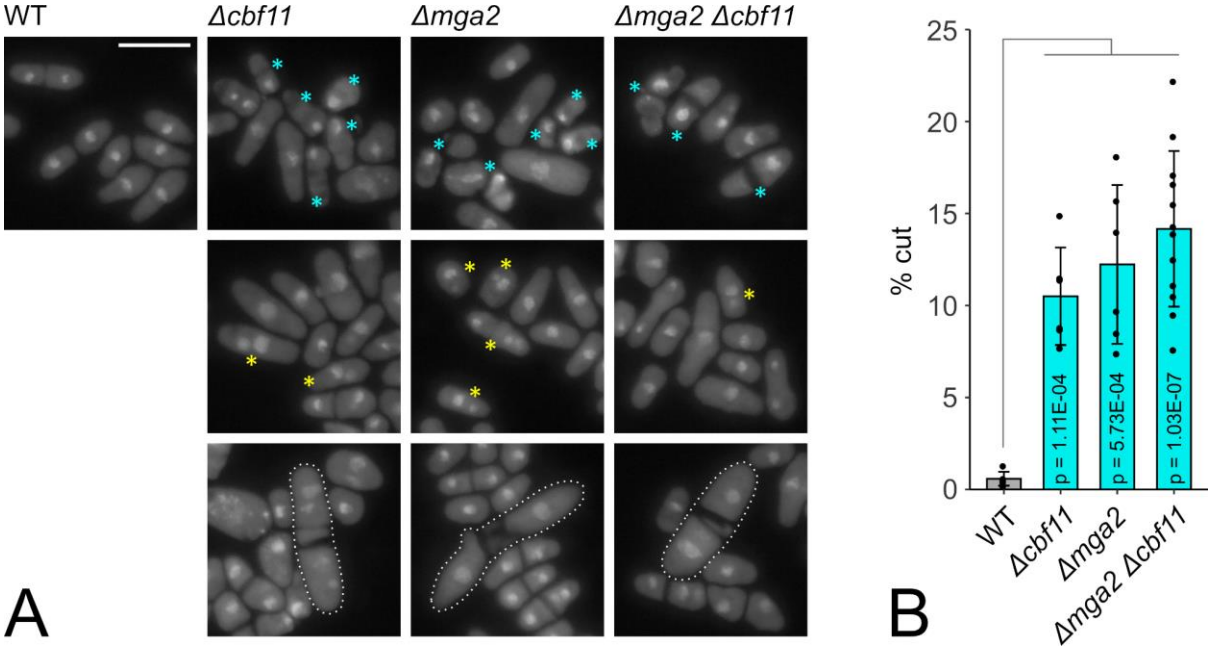

Figure 1: Cells lacking Cbf11 and/or Mga2 display similar, non-additive cellular defects. (A) Cells of the indicated genotypes were stained with DAPI to visualize nuclei. 'Cut' cells are marked with cyan asterisks (top row); cells with fragmented and/or diffuse nuclei are marked with yellow asterisks (middle row); filamentous cells with septation defects are highlighted with dotted outlines (bottom row). Representative images from 6 independent experiments are shown. Scale bar represents 10 µm. **(B)** Quantification of 'cut' phenotype occurrence. Mean ± SD values, as well as individual data points for ≥6 independent experiments are shown. Significance was determined by a Welch Two Sample t-test.

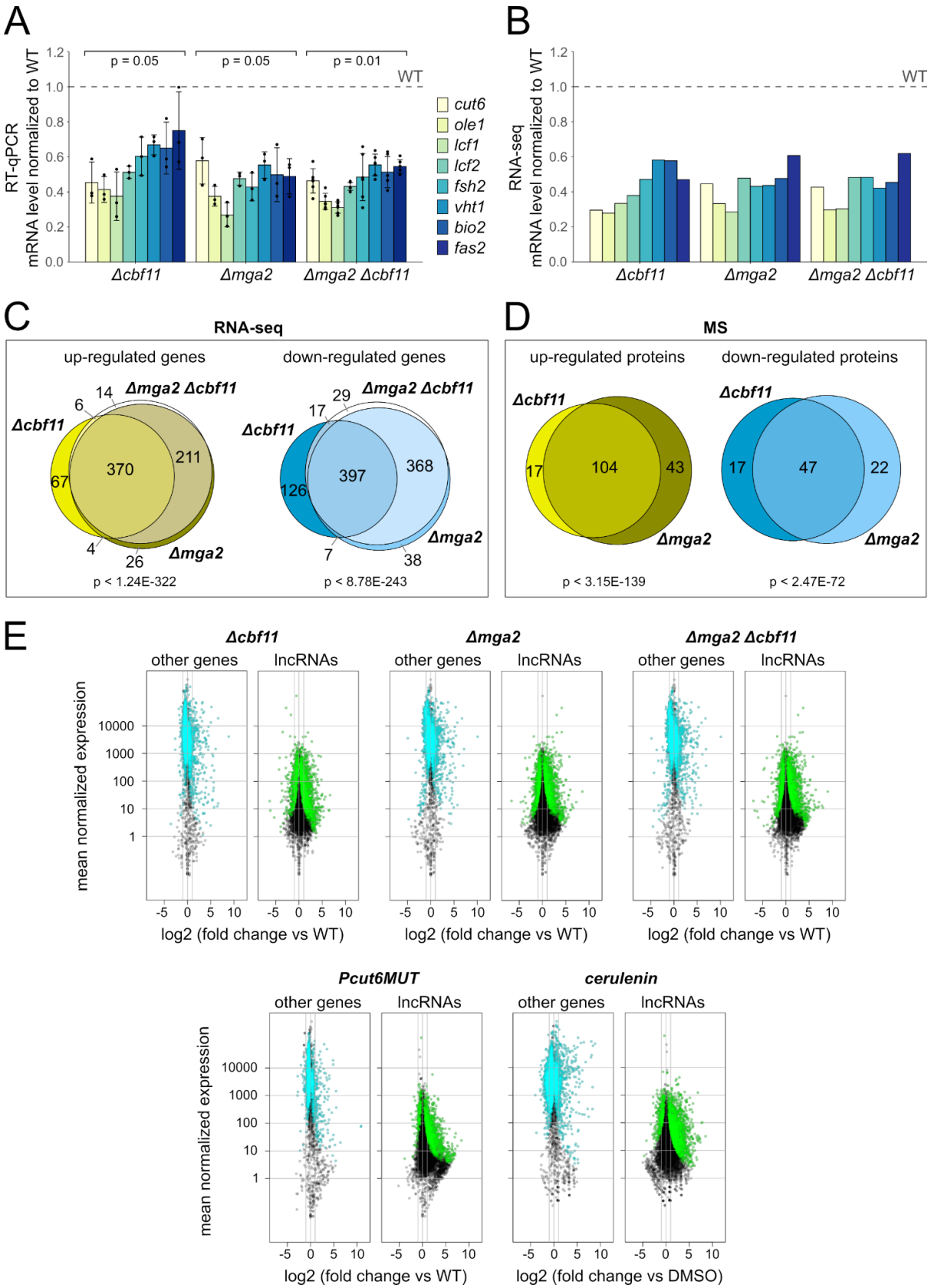

Figure 2: The absence of Cbf11 and/or Mga2 results in similar transcriptome and proteome changes. RT-qPCR **(A)** and RNA-seq **(B)** show that lipid metabolism genes are downregulated in *Δcbf11* and/or *Δmga2* mutants and this effect is not additive in the double deletion mutant. Means

values ± SD, as well as individual data points for ≥3 independent experiments are shown in panel (A). Mean values of 3 independent RNA-seq experiments are shown in panel (B). Significance of changes was determined by a one-sided Mann-Whitney U test. Venn diagrams showing that the sets of genes **(C)** and proteins **(D)** expressed differentially in *Δcbf11* and/or *Δmga2* cells significantly overlap (Fisher's exact test of RNA-seq and MS proteomics results, respectively). Only protein-coding genes and proteins showing at least 1.5-fold or 2-fold and statistically significant change in expression compared to WT are included in panel (C) and (D), respectively. **(E)** Both genetic and chemical perturbation of lipid metabolism result in deregulation of the non-coding transcriptome. Gene expression was determined by RNA-seq and compared to WT. Three independent experiments were performed. For each gene, the magnitude of change in expression was plotted against its mean expression value across all samples. Statistically significant differentially expressed genes are shown in cyan (other genes) or green (lncRNAs). The two gray vertical lines indicate the interval of 2-fold up- or downregulation.

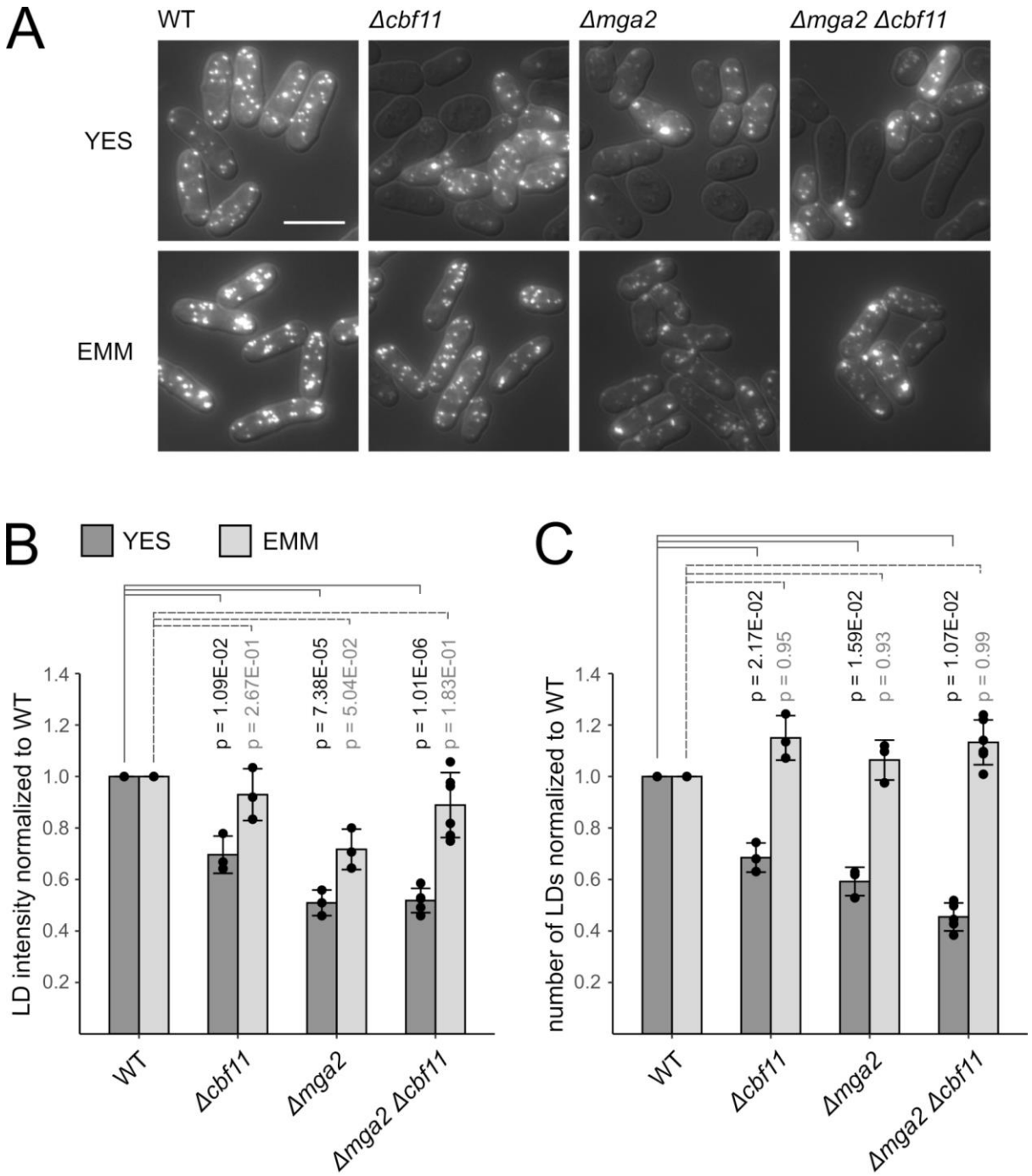

Figure 3: Cells lacking Cbf11 and/or Mga2 display nutrient-responsive decrease in lipid droplet (LD) content. (A) Cells of the indicated genotypes were stained with BODIPY 493/503 to visualize neutral lipids. Note the heterogeneity in LD content in *Δcbf11* and/or *Δmga2* mutants grown in the complex YES medium. The aberrant LD content is largely suppressed when cells are grown in the minimal EMM medium. Representative microscopic images from 3 independent experiments are shown. DIC overlay is shown to mark cell boundaries. Scale bar represents 10 µm. **(B, C)** Quantification of LD staining intensity and LD numbers per unit of cell volume. Mean ± SD values, as well as individual data points for ≥3 independent experiments are shown. Significance was determined by a Welch Two Sample t-test.

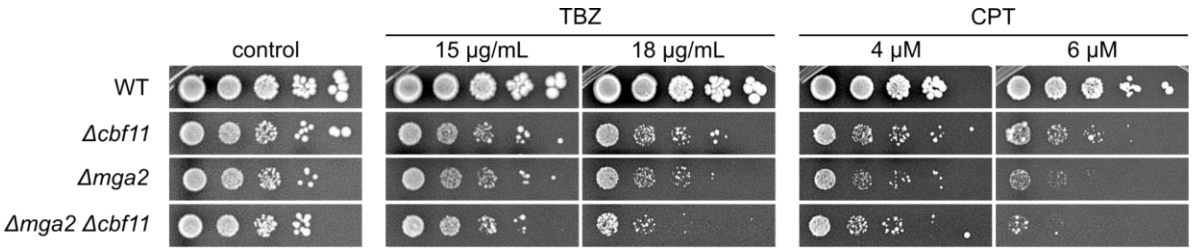

Figure 4: Cells lacking Cbf11 and/or Mga2 are sensitive to thiabendazole (TBZ) and camptothecin (CPT). Ten-fold serial dilutions of cultures of the indicated genotypes were plated on YES medium containing TBZ or CPT. Representative images from 2 independent experiments are shown.

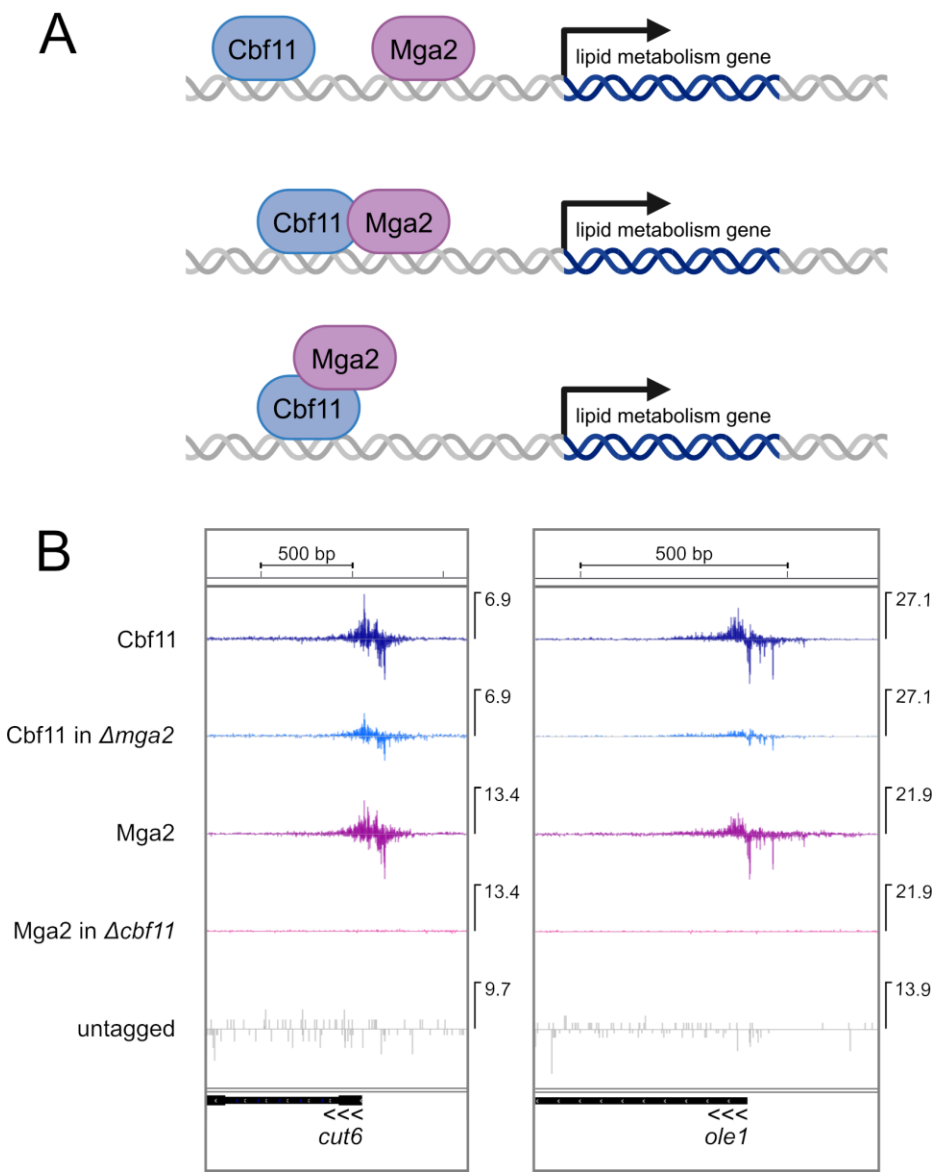

Figure 5: Mga2 binds to DNA in a Cbf11-dependent manner. (A) Scheme of three considered DNA binding regimes of Cbf11 and Mga2. See the main text for more detailed description. Image created with BioRender.com. **(B)** *In vivo* binding of Cbf11 and Mga2 TAP-tagged proteins to the promoters of selected lipid metabolism genes was analyzed by ChIP-nexus. Mean strand-specific coverage profile of 3 independent experiments for Cbf11 and Mga2 in the indicated genetic backgrounds, and a strand-specific coverage profile for untagged WT cells (negative control) are visualized in the Integrated Genome Viewer (IGV; Broad Institute). Gene orientation is indicated by three arrowheads; the maximum Y-axis value for each track is indicated on the right side of each panel.

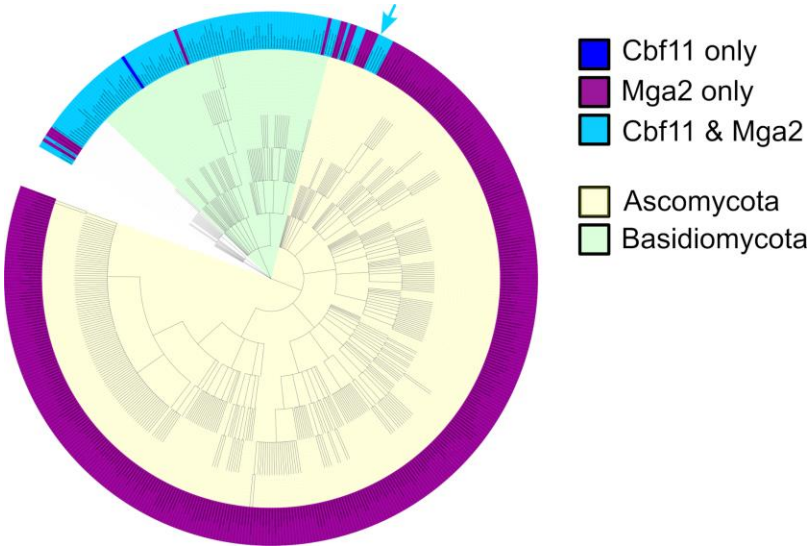

Figure 6: Phylogenetic distribution of Cbf11 and Mga2 homologs in Fungi. In the phylum Basidiomycota, members of the Cbf11 and Mga2 families are found together in almost all species. However, in the phylum Ascomycota, Cbf11 homologs are typically absent, except for the Taphrinomycotina group to which the fission yeasts belong (*S. pombe* position indicated with a light blue arrow). The taxonomy of some fungal species is uncertain (white part of the tree). Image created with iTOL v6**.**

SUPPLEMENTARY FIGURES

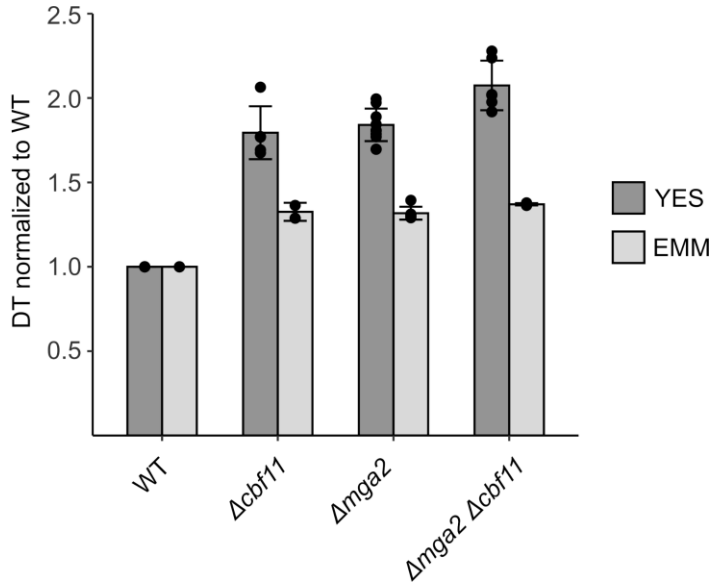

Supplementary Figure S1: The *Δcbf11* and *Δmga2* mutants show similar, non-additive growth defects. These defects are partially suppressed in the EMM minimal medium. Mean ± SD values, as well as individual data points for ≥2 independent experiments are shown.

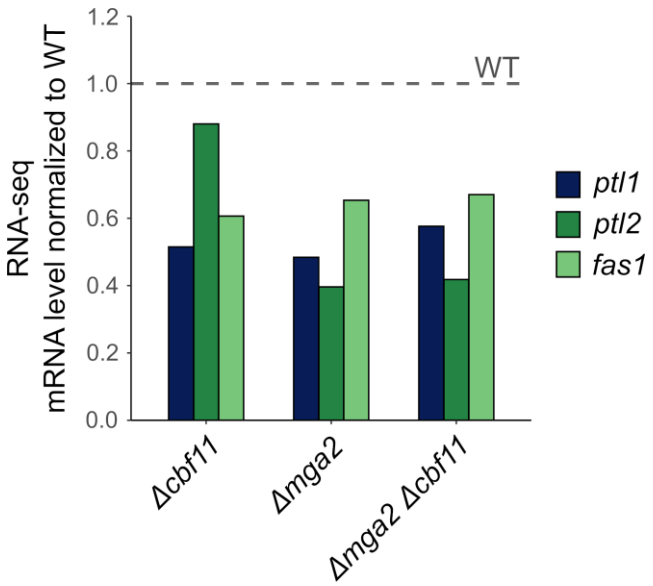

Supplementary Figure S2: RNA-seq shows non-additive decrease in transcript level of lipid metabolism genes in *Δmga2 Δcbf11* cells. The *ptl1* and *ptl2* genes encode triacylglycerol lipases, the *fas1* gene encodes the fatty acid synthase alpha subunit. Mean values for 3 independent experiments are shown.

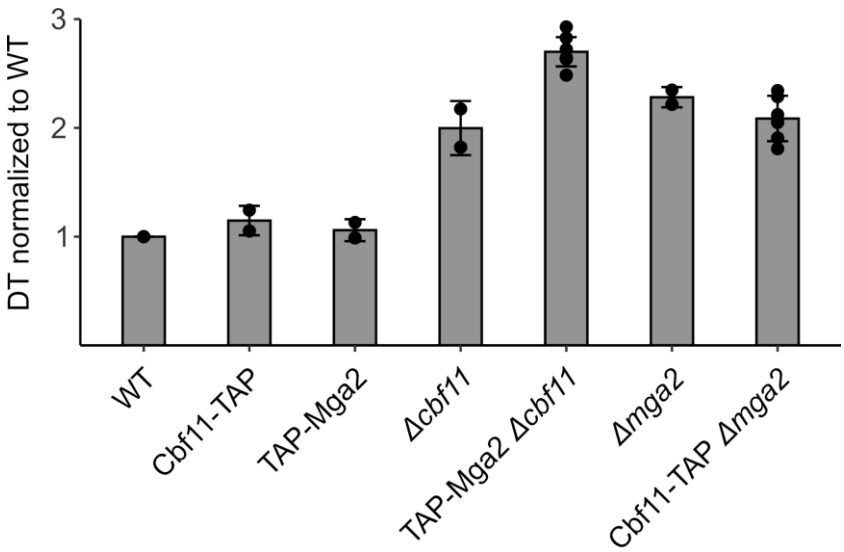

Supplementary Figure S3: The doubling times of *cbf11* and *mga2* knock-outs and scarless knock-ins. Mean ± SD values, as well as individual data points for ≥2 independent experiments are shown.

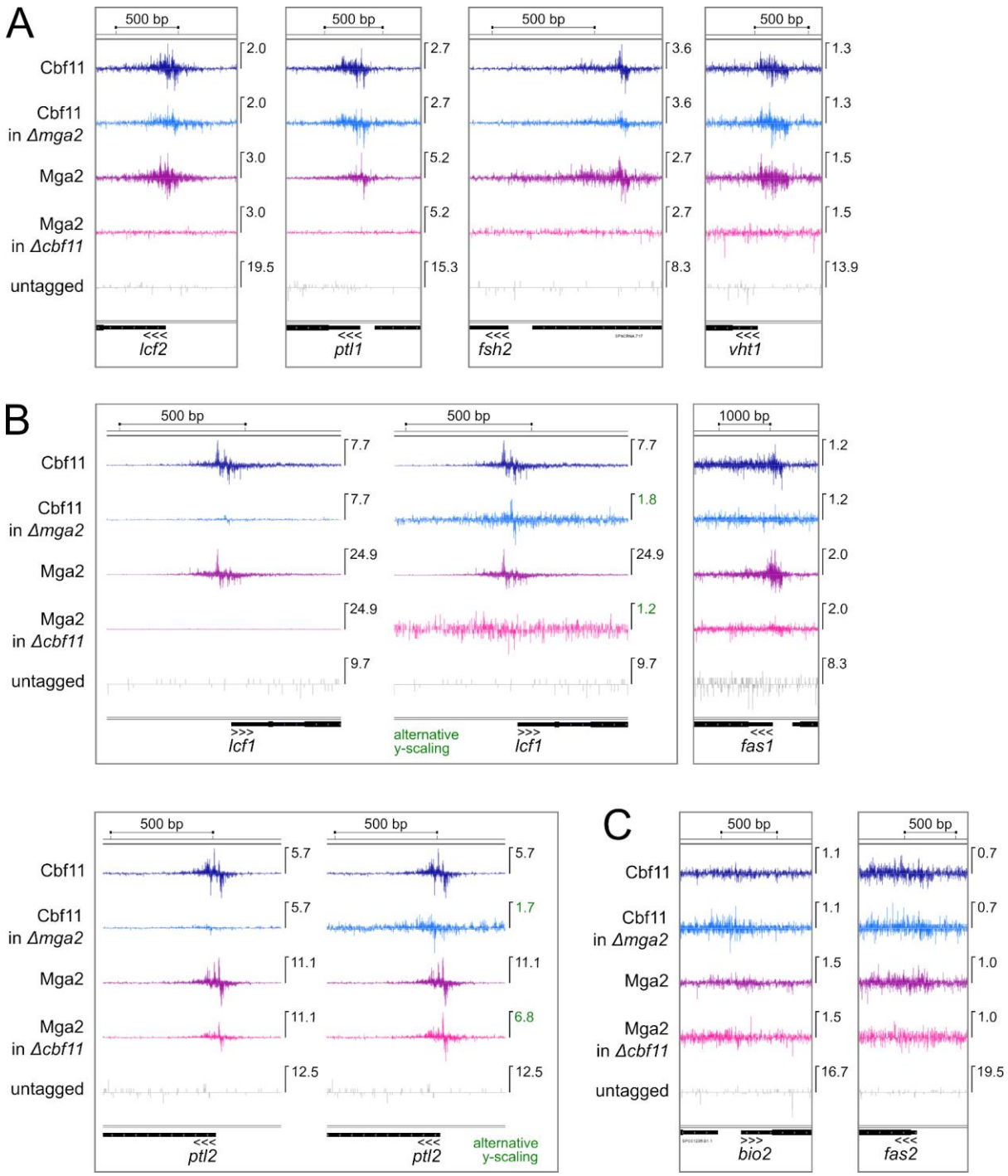

Supplementary Figure S4: ChIP-nexus analysis of Cbf11 and Mga2 binding to promoters of lipid metabolism genes. (A) Promoters to which both Cbf11 and Mga2 bind, and the binding is Cbf11-dependent. **(B)** Promoters where binding shows varying dependence on Cbf11 and/or Mga2. **(C)** Control loci with no binding. Mean strand-specific coverage profile of 3 independent experiments for Cbf11 and Mga2 in the indicated genetic backgrounds, and a strand-specific coverage profile for untagged WT cells (negative control) are visualized in the Integrated Genome Viewer (IGV; Broad Institute). Gene orientation is indicated by three arrowheads; the maximum Y-axis value for each track is indicated on the right side of each panel.

SUPPLEMENTARY MATERIAL

Text S1: *TAP-mga2 template for HR**

SacI - *mga2* 5' upstream - *mga2* 5'UTR - *NotI* - TAP (w/o STOP codon) - *XbaI* - linker - *PstI* - *mga2* ORF with silent point mutation * (C→A) - *XhoI*

GAGCTCGGGGGTCCAAGAGCAAATGTTGCAAGTGCTGCGAAATTTTACATGTCAGAAAGAAGAAAGCGTGG
ATTTTCTTTTGAAAATGGTTCCTATGGAGTTGTTAGCAAAAATTTTGCTTGAAAAATTAGAAAGTAAAAATCCT
ATCCTAATTGAACCCAGTATTTACATTTTGGTGCACATCGCTGCCAGCGATGGTGAGCTTAGGGATTCTATCC
TAAGGCAAACCAAACTACTACTATTGGTGAAGGAAATTATGCTACAAGAAGCACAACGTCTCAAGCCCGAGC
AAATGTCCACAAATGTGTCATCTCCGGAAAGTGACAGTGAAATGGATTTGCAAGAAGATGATTTTGATAGGG
AAATGCGTCCTCCTTTCGATATTTATGAAGAGGACACTTATGAACCAAACTCCGAAATTCTGTTGGCCGGAAT
TTGGCTCTGTATTAACATTCTATGGCCCAAACAATGTACATCTCCAAGCCAGGAAGATAAGGAAAGAGCAAG
TATCTTACAAAATCTCGGATTTGGAGAATGTTTGCAGATGCTACAAAATCACTCATCTCCTGATGTAAGGGAA
CGTGTCAAAGATGCCTTGATGTACATCAATGTAACCGATTAATTTCTATTACGCTTTTCCGTTGTCTTTGCCGA
CTTGATTGGAACAGTCTAACAAATCGGAGCCATTTTCGCATTTAGTATTTCTGTATGTATAAATGTGTGCACAA
CTCTTGCAGCTGAAGTTAACAGGTTGTTGGATTGAAGTACTTTGAGAATGATCGTATATAAAAAGATTTAATG
ATTTATCAAAACGAATAAAATAAGTATTATGAACATTCAACTTATATGTATGCGGGATAGTGTAAAAACCTATT
TAACATTGTAAAAATTTTTTAAGGAAAGTTGTACTTTGACAAGAACAATTTCATTTACATGTATTCTACTAAATT
TATCAGAATGTTGGGAATTTTTTTGTTGGTATATAATGCCGAAAGGAAATTAATCGAATATGAAGAAAGTGGC
GGAACTAAAAAACAAAACCCACAAACTAATTATTTAAATAAATATAACATAATAACTTGTTAAAATAAGAGTAAT
ACTAGAGAATGTGTGCTCAAGTGGAAAGCATGTAATACTTGCACAACGTGATGGAAGAGATTAGTGTAGTAG
CGCAGCGACAGCTTCCAACAACCAACTAATCGAGGAGGAAAGCAAAAGTGAGAATTGAAAAGAAGTAGTAC
ATTAAAGACCTTTAAATTCTTTGAAAGAATTGCCTTTATAAAGGTAGTCTATTGCATTTCAAAGTACTCTCAAG
GCGGCCGCATGAAGCGACGATGGAAAAAGAATTTCATAGCCGTCTCAGCAGCCAACCGCTTTAAGAAAATC
TCATCCTCCGGGGCACTTGATTATGGTACCCCAACTACTGCTTCTGAAAATCTATATTTTCAAGGTGAACTAA
AAACTGCTGCTTTGGCTCAACATGCGATTAAGGGTGAAGCTCAAAAACTTAATGACTCTCAAGCTCCAAAAG
CTGATGCGCAACAAAATAACTTCAACAAAGATCAACAAAGCGCCTTCTATGAAATCTTGAACATGCCTAACTT
AAACGAAGCGCAACGTAACGGCTTCATTCAAAGTCTTAAAGACGACCCAAGCCAAAGCACTAACGTTTTAGG
TGAAGCTAAAAAATTAAACGAATCTCAAGCACCGAAAGCTGATAACAATTTCAACAAAGAACAACAAAATGCT
TTCTATGAAATCTTGAATATGCCTAACTTAAACGAAGAACAACGCAATGGTTTCATCCAAAGCTTAAAAGATG
ACCCAAGCCAAAGTGCTAACCTATTGTCAGAAGCTAAAAAGTTAAATGAATCTCAAGCACCGAAAGCGGATA
ACAAATTCAACAAAGAACAACAAAATGCTTTCTATGAAATCTTACATTTACCTAACTTAAACGAAGAACAACGC
AATGGTTTCATCCAAAGCCTAAAAGATGACCCAAGCCAAAGCGCTAACCTTTTAGCAGAAGCTAAAAAGCTA
AATGATGCTCAAGCACCAAAAGCTGACAACAAATTCAACAAAGAACAACAAAATGCTTTCTATGAAATTTTAC
ATTTACCTAACTTAACTGAAGAACAACGTAACGGCTTCATCCAAAGCCTTAAAGACGATCCTTCGGTGAGCAA
AGAATCTAGAGGTTCTGGTGGTTCTGGTCTGCAGATGAATTTAGAATTTTCTTTTGGAAATTTGATCGCCAAA
AATACAGAGAATTCGACTAAGGAAGAAGGAACTTGGGAAGTAAACAAGCTCATGAAATTTAGTTCAGAGGAG
GGGAGGTCTTCCTCTGATGATTATATGTTTTCCTCTCCCGATTTTGAAAAAGCCGGAAACGGCGATGCAGAA
ATGCGTGAATTTTTTAACTTCGATGGATTGCCGGATCAAGGTCTAAATTTGCCTAGTATAGCTCCTCCGTCTT
TATCCCATGCCAGTTCACCTAACTTATCGAATTCACAAGATGAAGCGGAATGTTTACCGTCTGATCGTCAGCA
AGACTACATCAATCCTAGTTTGCATTTGAACAGAACGGTGTTTCCTACTCCGCAACATTCTATTTCTGATGCT
AATTTTCTAGCTAATACCGTTGATCAACCTTTGGGAGATAATCCCATGTTTGGAGAGTCGGATGTTTATCTTTT
AAAAATGGATCCTATGAAACAAGCACCTTATGAAGCTGGATTTAATTCTGTAAAGTCATCGGGCGCCATCGAA
GATCCATTACAGTTTAGACAGCCGATTACCATGTTGGAAACTCCCTTCAACGAATCTATTAATACTCTTACGC
CATATGCCGAAGATTATGCATTTTCCTCTTTAAATACGTCTGCACCGCCTCTTTCTAATAAGGAGTACGCGTT
CTCAGTTAATCATTTACCAGCTATCAATGAGCACAAATGGAAATCTCGGGTGGAAACTAACATGCTTTTTGAG
TTGCGGATCAAGAGCAACGATAATCAAAGTGTTCCGTTTGAATATCTTCGCTTGCCAAGTTGGGCTCACCGT
GAAGACAAAAAGCGTTCTTCGAAACCTCAGCCTTTGCAACCCGATCCGGAGACCGTCATTCATCTTGTACCT
ACCGTTCTTGCAGGTGACAAAAGCTCAGTTGTTAAGACTTGCTGTACTCGCTGTTTACTTCGAGAAAGGAAG
CGCAATGCTCGATCTCAAGCAACAAAGGATGCTTGTATGCCTAACTATACTAAACTGAAGGCTTATGAGCGT
AACATGACTGATGCCTCTCCCGAAGAAAAGCAGCAGTTCAGGATCAAGCTCTTAAATCAATTTCCCAAACTTG
AAGACATAGATGAAGATAGAATGATAATGGTTTTTACTGGACCTGAGTACGTTCGTTTGCAATTGGATGGAAA
TGAAAGAGTTGCTCACATCAATGCACGGATTACATGTTACTCGTCTCATCAATCATGCCCTTACTTTCACATC
ATATGGGACTTATACTCCATGTCACGTTTGGTGGATCGTCTTGTTTTTCCAGAGCCTGTTACCGTTCTTGATG
ATCATAAAAGTAGAAATCTTACGAAATCAGAAAAGACTGGTAAGAGCAATTCTCAACAAGCTCCTTCAAACCA
TGTTCTTTCTAAAAGCAATACTGTCCCCAATCTTGTCACTGGTTTCCCTACCCGTTCAGATAATCCACCAAAT
GAAAAGCGTCGTCGAACATCCTCGAG

REFERENCES

Beckley, J. R., Chen, J.-S., Yang, Y., Peng, J. and Gould, K. L. (2015). A Degenerate Cohort of Yeast Membrane Trafficking DUBs Mediates Cell Polarity and Survival. *Mol. Cell. Proteomics* **14**, 3132–41.

Bhattacharya, S., Shcherbik, N., Vasilescu, J., Smith, J. C., Figeys, D. and Haines, D. S. (2009). Identification of Lysines within Membrane-Anchored Mga2p120 that Are Targets of Rsp5p Ubiquitination and Mediate Mobilization of Tethered Mga2p90. *J. Mol. Biol.* **385**, 718–725.

Burr, R., Stewart, E. V., Shao, W., Zhao, S., Hannibal-Bach, H. K., Ejsing, C. S. and Espenshade, P. J. (2016). Mga2 Transcription Factor Regulates an Oxygen-responsive Lipid Homeostasis Pathway in Fission Yeast. *J. Biol. Chem.* **291**, 12171–83.

Burr, R., Stewart, E. V. and Espenshade, P. J. (2017). Coordinate Regulation of Yeast Sterol Regulatory Element-binding Protein (SREBP) and Mga2 Transcription Factors. *J. Biol. Chem.* **292**, 5311–5324.

Carpy, A., Krug, K., Graf, S., Koch, A., Popic, S., Hauf, S. and Macek, B. (2014). Absolute proteome and phosphoproteome dynamics during the cell cycle of fission yeast. *Mol. Cell. Proteomics*.

Chellappa, R., Kandasamy, P., Oh, C. S., Jiang, Y., Vemula, M. and Martin, C. E. (2001). The membrane proteins, Spt23p and Mga2p, play distinct roles in the activation of Saccharomyces cerevisiae OLE1 gene expression. Fatty acid-mediated regulation of Mga2p activity is independent of its proteolytic processing into a soluble transcription act. *J. Biol. Chem.* **276**, 43548–56.

Cox, J. and Mann, M. (2008). MaxQuant enables high peptide identification rates, individualized p.p.b.-range mass accuracies and proteome-wide protein quantification. *Nat. Biotechnol.* **26**, 1367–72.

Cox, J., Hein, M. Y., Luber, C. A., Paron, I., Nagaraj, N. and Mann, M. (2014). Accurate proteome-wide label-free quantification by delayed normalization and maximal peptide ratio extraction, termed MaxLFQ. *Mol. Cell. Proteomics* **13**, 2513–26.

Foo, S., Cazenave-Gassiot, A., Wenk, M. R. and Oliferenko, S. (2023). Diacylglycerol at the inner nuclear membrane fuels nuclear envelope expansion in closed mitosis. *J. Cell Sci.* **136**,.

Gregan, J., Rabitsch, P. K., Rumpf, C., Novatchkova, M., Schleiffer, A. and Nasmyth, K. (2006). High-throughput knockout screen in fission yeast. *Nat. Protoc.* **1**, 2457–64.

Hapala, I., Griac, P. and Holic, R. (2020). Metabolism of Storage Lipids and the Role of Lipid Droplets in the Yeast Schizosaccharomyces pombe. *Lipids* **55**, 513–535.

Hartmuth, S. and Petersen, J. (2009). Fission yeast Tor1 functions as part of TORC1 to control mitotic entry through the stress MAPK pathway following nutrient stress. *J. Cell Sci.* **122**, 1737–46.

He, Q., Johnston, J. and Zeitlinger, J. (2015). ChIP-nexus enables improved detection of in vivo transcription factor binding footprints. *Nat. Biotechnol.* **33**, 395–401.

Hebert, A. S., Richards, A. L., Bailey, D. J., Ulbrich, A., Coughlin, E. E., Westphall, M. S. and Coon, J. J. (2014). The one hour yeast proteome. *Mol. Cell. Proteomics* **13**, 339–47.

Holič, R., Pokorná, L. and Griač, P. (2020). Metabolism of phospholipids in the yeast Schizosaccharomyces pombe. *Yeast* **37**, 73–92.

Hughes, A. L., Todd, B. L. and Espenshade, P. J. (2005). SREBP pathway responds to sterols and functions as an oxygen sensor in fission yeast. *Cell* **120**, 831–42.

Hughes, C. S., Moggridge, S., Müller, T., Sorensen, P. H., Morin, G. B. and Krijgsveld, J. (2019). Single-pot, solid-phase-enhanced sample preparation for proteomics experiments. *Nat. Protoc.* **14**, 68–85.

Jiang, Y., Vasconcelles, M. J., Wretzel, S., Light, A., Martin, C. E. and Goldberg, M. A. (2001). MGA2 is involved in the low-oxygen response element-dependent hypoxic induction of genes in Saccharomyces cerevisiae. *Mol. Cell. Biol.* **21**, 6161–9.

Kettenbach, A. N., Deng, L., Wu, Y., Baldissard, S., Adamo, M. E., Gerber, S. A. and Moseley, J. B. (2015). Quantitative phosphoproteomics reveals pathways for coordination of cell growth and division by the conserved fission yeast kinase pom1. *Mol. Cell. Proteomics* **14**, 1275–87.

Koch, A., Krug, K., Pengelley, S., Macek, B. and Hauf, S. (2011). Mitotic substrates of the kinase aurora with roles in chromatin regulation identified through quantitative phosphoproteomics of fission yeast. *Sci. Signal.* **4**, rs6.

Køhler, J. B., Tammsalu, T., Jørgensen, M. M., Steen, N., Hay, R. T. and Thon, G. (2015). Targeting of SUMO substrates to a Cdc48-Ufd1-Npl4 segregase and STUbL pathway in fission yeast. *Nat. Commun.* **6**, 8827.

Kwon, E. G., Laderoute, A., Chatfield-Reed, K., Vachon, L., Karagiannis, J. and Chua, G. (2012). Deciphering the transcriptional-regulatory network of flocculation in Schizosaccharomyces pombe. *PLoS Genet.* **8**, e1003104.

Larochelle, M., Bergeron, D., Arcand, B. and Bachand, F. (2019). Proximity-dependent biotinylation mediated by TurboID to identify protein-protein interaction networks in yeast. *J. Cell Sci.* **132**,.

Lee, C.-Y. S., Yeh, T.-L., Hughes, B. T. and Espenshade, P. J. (2011). Regulation of the Sre1 hypoxic transcription factor by oxygen-dependent control of DNA binding. *Mol. Cell* **44**, 225–34.

Mak, T., Jones, A. W. and Nurse, P. (2021). The TOR-dependent phosphoproteome and regulation of cellular protein synthesis. *EMBO J.* **40**, e107911.

Makarova, M., Gu, Y., Chen, J.-S., Beckley, J. R., Gould, K. L. and Oliferenko, S. (2016). Temporal Regulation of Lipin Activity Diverged to Account for Differences in Mitotic Programs. *Curr. Biol.* **26**, 237–243.

Marešová, A., Oravcová, M., Rodríguez-López, M., Hradilová, M., Zemlianski, V., Häsler, R., Hernández, P., Bähler, J. and Převorovský, M. (2024). Critical importance of DNA binding for CSL protein functions in fission yeast. *J. Cell Sci.* jcs.261568.

Marguerat, S., Schmidt, A., Codlin, S., Chen, W., Aebersold, R. and Bähler, J. (2012). Quantitative analysis of fission yeast transcriptomes and proteomes in proliferating and quiescent cells. *Cell* **151**, 671–83.

Meyers, A., Del Rio, Z. P., Beaver, R. A., Morris, R. M., Weiskittel, T. M., Alshibli, A. K., Mannik, J., Morrell-Falvey, J. and Dalhaimer, P. (2016). Lipid Droplets Form from Distinct Regions of the Cell in the Fission Yeast Schizosaccharomyces pombe. *Traffic* **17**, 657–69.

Meyers, A., Chourey, K., Weiskittel, T. M., Pfiffner, S., Dunlap, J. R., Hettich, R. L. and Dalhaimer, P. (2017). The protein and neutral lipid composition of lipid droplets isolated from the fission yeast, Schizosaccharomyces pombe. *J. Microbiol.* **55**, 112–122.

Oravcová, M., Teska, M., Půta, F., Folk, P. and Převorovský, M. (2013). Fission yeast CSL proteins function as transcription factors. *PLoS One* **8**, e59435.

Pancaldi, V., Saraç, O. S., Rallis, C., McLean, J. R., Převorovský, M., Gould, K., Beyer, A. and Bähler, J. (2012). Predicting the fission yeast protein interaction network. *G3 (Bethesda).* **2**, 453–67.

Petersen, J. and Russell, P. (2016). Growth and the Environment of Schizosaccharomyces pombe. *Cold Spring Harb. Protoc.* **2016**, pdb.top079764.

Převorovský, M., Půta, F. and Folk, P. (2007). Fungal CSL transcription factors. *BMC Genomics* **8**, 233.

Převorovský, M., Groušl, T., Staňurová, J., Ryneš, J., Nellen, W., Půta, F. and Folk, P. (2009). Cbf11 and Cbf12, the fission yeast CSL proteins, play opposing roles in cell adhesion and coordination of cell and nuclear division. *Exp. Cell Res.* **315**, 1533–47.

Převorovský, M., Atkinson, S. R., Ptáčková, M., McLean, J. R., Gould, K., Folk, P., Půta, F. and Bähler, J. (2011). N-termini of fungal CSL transcription factors are disordered, enriched in regulatory motifs and inhibit DNA binding in fission yeast. *PLoS One* **6**, e23650.

Převorovský, M., Oravcová, M., Tvarůžková, J., Zach, R., Folk, P., Půta, F. and Bähler, J. (2015). Fission Yeast CSL Transcription Factors: Mapping Their Target Genes and Biological Roles. *PLoS One* **10**, e0137820.

Převorovský, M., Oravcová, M., Zach, R., Jordáková, A., Bähler, J., Půta, F. and Folk, P. (2016). CSL protein regulates transcription of genes required to prevent catastrophic mitosis in fission yeast. *Cell Cycle* **15**, 3082–3093.

Princová, J., Schätz, M., Ťupa, O. and Převorovský, M. (2019). Analysis of Lipid Droplet Content in Fission and Budding Yeasts using Automated Image Processing. *J. Vis. Exp.* 1–9.

Princová, J., Salat-Canela, C., Daněk, P., Marešová, A., de Cubas, L., Bähler, J., Ayté, J., Hidalgo, E. and Převorovský, M. (2023). Perturbed fatty-acid metabolism is linked to localized chromatin hyperacetylation, increased stress-response gene expression and resistance to oxidative stress. *PLoS Genet.* **19**, e1010582.

Rappsilber, J., Mann, M. and Ishihama, Y. (2007). Protocol for micro-purification, enrichment, pre-fractionation and storage of peptides for proteomics using StageTips. *Nat. Protoc.* **2**, 1896–906.

Rodríguez-López, M., Cotobal, C., Fernández-Sánchez, O., Borbarán Bravo, N., Oktriani, R., Abendroth, H., Uka, D., Hoti, M., Wang, J., Zaratiegui, M., et al. (2016). A CRISPR/Cas9-based method and primer design tool for seamless genome editing in fission yeast. *Wellcome open Res.* **1**, 19.

Selicky, T., Jurcik, M., Mikolaskova, B., Pitelova, A., Mayerova, N., Kretova, M., Osadska, M., Jurcik, J., Holic, R., Kohutova, L., et al. (2022). Defining the Functional Interactome of Spliceosome-Associated G-Patch Protein Gpl1 in the Fission Yeast Schizosaccharomyces pombe. *Int. J. Mol. Sci.* **23**,.

Skruzny, M., Pohl, E. and Abella, M. (2019). FRET Microscopy in Yeast. *Biosensors* **9**, 1–17.

Strachan, J., Leidecker, O., Spanos, C., Le Coz, C., Chapman, E., Arsenijevic, A., Zhang, H., Zhao, N., Spoel, S. H. and Bayne, E. H. (2023). SUMOylation regulates Lem2 function in centromere clustering and silencing. *J. Cell Sci.* **136**,.

Takemoto, A., Kawashima, S. A., Li, J.-J., Jeffery, L., Yamatsugu, K., Elemento, O. and Nurse, P. (2016). Nuclear envelope expansion is crucial for proper chromosomal segregation during a closed mitosis. *J. Cell Sci.* **129**, 1250–9.

Torres-Garcia, S., Di Pompeo, L., Eivers, L., Gaborieau, B., White, S. A., Pidoux, A. L., Kanigowska, P., Yaseen, I., Cai, Y. and Allshire, R. C. (2020). SpEDIT: A fast and efficient CRISPR/Cas9 method for fission yeast. *Wellcome open Res.* **5**, 274.

Tyanova, S., Temu, T., Sinitcyn, P., Carlson, A., Hein, M. Y., Geiger, T., Mann, M. and Cox, J. (2016). The Perseus computational platform for comprehensive analysis of (prote)omics data. *Nat. Methods* **13**, 731–40.

Vasconcelles, M. J., Jiang, Y., McDaid, K., Gilooly, L., Wretzel, S., Porter, D. L., Martin, C. E. and Goldberg, M. A. (2001). Identification and characterization of a low oxygen response element involved in the hypoxic induction of a family of Saccharomyces cerevisiae genes. Implications for the conservation of oxygen sensing in eukaryotes. *J. Biol. Chem.* **276**, 14374–84.

Vishwanatha, A., Princová, J., Hohoš, P., Zach, R. and Převorovský, M. (2023). Altered cohesin dynamics and H3K9 modifications contribute to mitotic defects in the cbf11Δ lipid metabolism mutant. *J. Cell Sci.*

Yam, C., He, Y., Zhang, D., Chiam, K.-H. and Oliferenko, S. (2011). Divergent strategies for controlling the nuclear membrane satisfy geometric constraints during nuclear division. *Curr. Biol.* **21**, 1314–9.

Yanagida, M. (1998). Fission yeast cut mutations revisited: control of anaphase. *Trends Cell Biol.* **8**, 144–9.

Zach, R. and Převorovský, M. (2018). The phenomenon of lipid metabolism “cut” mutants. *Yeast* **35**, 631–637.

Zach, R., Tvarůžková, J., Schätz, M., Ťupa, O., Grallert, B. and Převorovský, M. (2018). Mitotic defects in fission yeast lipid metabolism “cut” mutants are suppressed by ammonium chloride. *FEMS Yeast Res.* **18**, 1–7.

Zemlianski V, Marešová A, Princová J, Holič R, Häsler R, Ramos del Río MJ, Lhoste L, Zarechyntsava M, Převorovský M. (2023). Nitrogen availability and TOR signalling are important for preventing catastrophic mitosis in fission yeast. bioRxiv doi: 10.1101/2023.12.25.573293

Zhang, S., Burkett, T. J., Yamashita, I. and Garfinkel, D. J. (1997). Genetic redundancy between SPT23 and MGA2: regulators of Ty-induced mutations and Ty1 transcription in Saccharomyces cerevisiae. *Mol. Cell. Biol.* **17**, 4718–29.

Zhang, S., Skalsky, Y. and Garfinkel, D. J. (1999). MGA2 or SPT23 is required for transcription of the delta9 fatty acid desaturase gene, OLE1, and nuclear membrane integrity in Saccharomyces cerevisiae. *Genetics* **151**, 473–83.

Zielinska, D. F., Gnad, F., Schropp, K., Wiśniewski, J. R. and Mann, M. (2012). Mapping N-glycosylation sites across seven evolutionarily distant species reveals a divergent substrate proteome despite a common core machinery. *Mol. Cell* **46**, 542–8.